Journal of Materials Science and Chemical Engineering, 2025, 13(8), 66-85
https://www.scirp.org/journal/msce
ISSN Online: 2327-6053
ISSN Print: 2327-6045

Feasible Fabrication of Chitosan Capped Mesoporous Silica Nanoparticles as a Smart Mucoadhesive Drug Delivery Platform for Dexamethasone for Long Term Lung Treatment

Long-Siang Lee[1], Norman C.-R. Chen[2,3], Kevin C.-W. Wu[4*]

[1]Viterbi School of Chemical Engineering, University of Southern California, Los Angeles, CA
[2]Molecular Science and Technology Program, Taiwan International Graduate Program (TIGP), Academia Sinica, Taipei City
[3]International Graduate Program of Molecular Science and Technology (NTU-MST), NTU, Taipei City
[4]Department of Chemical Engineering, NTU, Taipei City
Email: *kevinwu@ntu.edu.tw

How to cite this paper: Lee, L.-S., Chen, N.C.-R. and Wu, K.C.-W. (2025) Feasible Fabrication of Chitosan Capped Mesoporous Silica Nanoparticles as a Smart Mucoadhesive Drug Delivery Platform for Dexamethasone for Long Term Lung Treatment. *Journal of Materials Science and Chemical Engineering*, **13**, 66-85.
https://doi.org/10.4236/msce.2025.138006

Received: July 8, 2025
Accepted: August 24, 2025
Published: August 27, 2025

Abstract

Among the carriers, mesoporous silica nanoparticles (MSN) were promising for drug carriers due to their biocompatibility and high porosity, thereby increasing the loading of therapeutic agents. Chitosan, a biocompatible polymer with a positive charge, was used to modify the MSN surface in order to achieve strong electrostatic mucoadhesion and further improve drug loading capacity and sustainable release profile. The MCM-41 type was prepared using a CTAB-templated sol-gel method. The SBA-15 type MSNs were prepared using the P123 surfactant template. MCM-41 was further aminated, then coated with chitosan via the crosslinking of glutaraldehyde. With an X-ray diffractometer, the hexagonal close-packed crystal structure of MSN was verified for MCM-41 and SBA-15. SEM demonstrated the particle morphology and distribution of MSNs. Fourier transform infrared spectroscopy measured vibration modes of alkyl, amine, hydroxyl, and silica functions, confirming the encapsulation of chitosan on the MCM-41 (MCM-41-CHIT) surface. The small dexamethasone was encapsulated in the chitosan capped MCM-41. The drug loading capacity of MCM-41-CHIT revealed 53.7%. The burst release of dexamethasone in the unmodified MSNs was noted, which showed 80% in 24 hours. On the other hand, drug release in MCM-41-CHIT showed constant and delayed release, which showed only 19.7% in 120 hours and a potential to last 55 days. In summary, this research established chitosan capped MCM-41 as a potentially efficient candidate for the mucoadhesive drug delivery system used in long-term treatment.

Keywords

Mesoporous Silica Nanoparticles, Chitosan, Mucoadhesion, Dexamethasone

1. Introduction

COVID-19 was a virus-induced lung disease that caused millions of deaths globally [1]. In the therapy trial study, the use of dexamethasone (DEX) daily for up to 10 days resulted in lower 28-day mortality among those severe hospitalized patients with intensive care [2] [3]. Dexamethasone is a corticosteroid, which worked on the immune system to help relieve swelling, redness, itching, and allergic reactions [2]-[4]. Oral and intravenous dexamethasone therapy in the long-term treatment course would cause systemic adverse effects [4]-[6]. Direct drug delivery to the airway or inhalation therapy was commonly used to treat lung diseases. Inhalation therapy was accessible to deliver the therapeutic drug to the lung mucosa and, therefore, could significantly reduce the drug's dose and further reduce its side effects.

A long-term release and high concentration of dexamethasone were required to cure the lung inflammatory disease [2] [3]. The control of release over a long period of time was an important factor to be taken into account for improving maximum treatment benefits. Thus, to reduce the adverse effects of the drug resulting from high dosage burst release, a sustainable drug delivery system should be designed with biocompatible nanomaterials.

For drug delivery purposes, the mechanism of mucoadhesion involves the attachment of a drug carrier system to the mucous membrane of a tissue [7]-[9]. The mucous membrane lining the respiratory system, including the nose, the larynx, the trachea and the lung, has a great surface area and plays a crucial role in the protection of the inhaled air [8] [10] [11]. Nanoparticle composites offered advantages in improving cell penetration and thus demonstrated a promising tool for treating lung diseases [12]-[14]. As delivered to the airway via inhalation, these nanoparticles could remain or penetrate the mucus layer through adhesion-mediated approaches.

Mesoporous silica nanoparticles (MSNs) with pore size 2 - 50 nm played an important role as a carrier in mucoadhesive delivery and control of drug release in pharmaceutical technology [15]-[17]. The benefits of utilizing MSNs in medical applications were enhanced drug bioavailability and reduced unwanted toxicity due to their modifiable surface, suitable nano-size, tunable pore size and chemical stability [15]-[17].

Chitosan, a derivative obtained from the deacetylation of chitin, has distinctive biological properties and has been widely used for sustained release and targeted preparations of drugs [18] [19]. Because the abundant amino groups of chitosan were protonated and positively charged, chitosan could effectively react with the negative charge of mucus gel [7] [8] [12] [18]. When chitosan-

based drug carriers were inhaled into the respiratory tract, the strong electrostatic adhesion of chitosan to the mucous membrane occurred [18] [19]. Chitosan with particular mucoadhesion ability could increase the retention time of the drug in the pulmonary mucosa, resulting in slow and cumulative release of the drug.

In this study, we proposed a simple and feasible method to fabricate an MSN and chitosan nano-composite for the construction of a mucoadhesive drug delivery platform. Firstly, MSNs in three biodegradable nanoparticle forms were synthesized by the use of tetraethyl orthosilicate (TEOS). Secondly, MSNs were modified with APTES. Aminated MSNs were capped with chitosan mediated by glutaraldehyde as a cross-linker. Subsequently, the nanoparticles' size, pore size, surface morphology and dexamethasone loading content were investigated. The cumulative drug release in physiological conditions was monitored.

2. Materials and Methods

2.1. Reagents and Apparatus

The experimental chemicals used were listed in Table 1.

2.2. Fabrication Method of Mesoporous Silica Nanoparticles (MSNs)

2.2.1. Synthesis of MCM-41

The experimental apparatus was set up and shown in Figure 1. CTAB (1g) was dissolved in a solution containing deionized water (480 mL) and 2N NaOH (3 mL). The mixed solution was treated with two different conditions: 1) stirred vigorously at 80˚C for 2 hours; 2) stirred vigorously at 60˚C for 1 hour. 98% TEOS (5 mL) was rapidly added to the above solutions, and the mixture was maintained at 80˚C /60˚C for 2 h/1 h until a white precipitate formed. After that, the products were obtained through centrifugation at 15,000 rpm for 10 min and rinsed with deionized water and 75% ethanol. Then the samples were vacuum-dried (60˚C, 24 h) to produce the as-synthesized MCM-41. Finally, the as-synthesized MCM-41 was calcined at 550˚C for 6 h to remove the surfactant template (CTAB), then the MSN sample was finally synthesized. The process of MCM-41 preparation was illustrated in Figure 2.

2.2.2. Synthesis of SBA-15

4g of P123 and 123 mL of HCl (pH = 3.00) were added to a two-neck bottle. The mixture was heated with an oil bath (650 rpm, 40˚C). When the solution turned

Table 1. Laboratory chemicals.

Dexamethasone sodium phosphate (DEX, ASTAR CHEMICAL)	Tetraethyl orthosilicate (TEOS, Tokyo Chemical Industry)	Cetyltrimethylammonium bromide (CTAB, Tokyo Chemical Industry)	3-Aminopropyl triethoxysilane (APTES, Tokyo Chemical Industry)
P123 (Sigma; 5800 g/mol, 1.11 g/mL)	Ammonium hydride (28%, SHOWA)	Chitosan (CHIT)	Phosphate buffer saline (PBS)
Glutaraldehyde	Glacial Acetic	NaOH	HCl

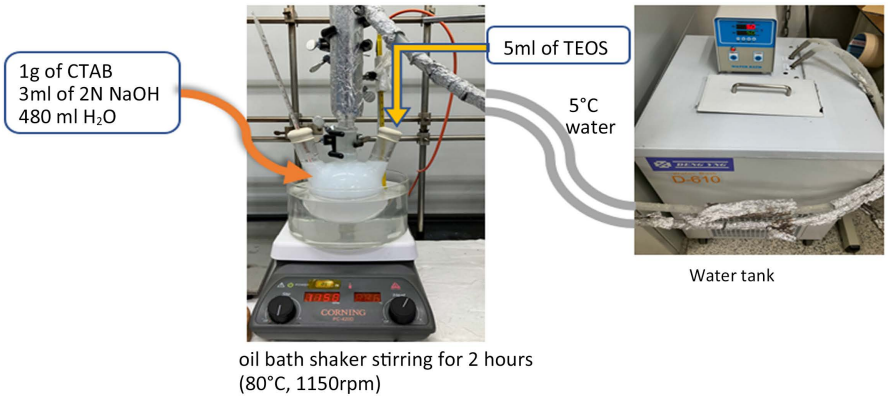

Figure 1. Experimental setup for MCM-41 synthesis.

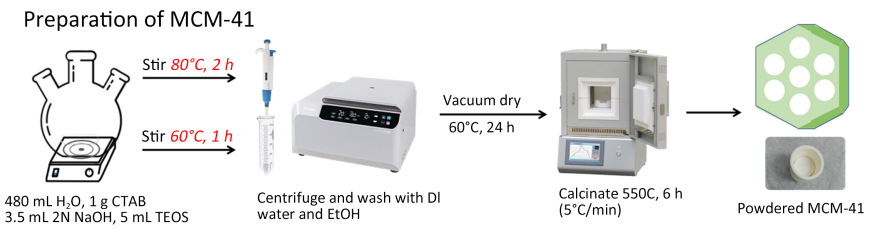

Figure 2. Schematic illustration of preparation of MCM-41.

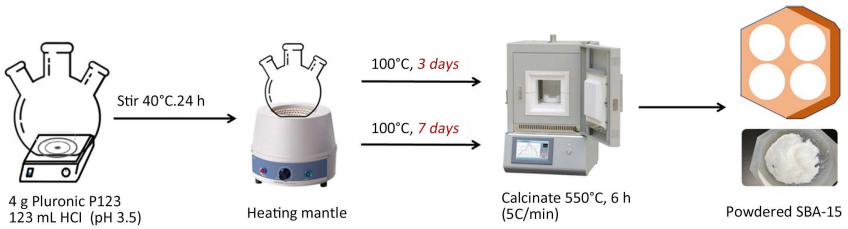

Figure 3. Schematic illustration of preparation of SBA-15.

clear, 98% TEOS (8 mL) was added with syringe. The mixture was stirred and heated with oil bath (1150 rpm, 40˚C, 24 h). Then, the two-neck bottle was transferred to a heating mantle and treated with two conditions: 1) 100˚C, 3 days; 2) 100˚C, 7 days. The solid sample retrieved after heating were vacuum dried (24 h) and calcinated (550˚C, 6 h). The process of SBA-15 synthesis was illustrated in Figure 3.

2.3. Functionalization of MCM-41 with APTES

MCM-41 was selected to proceed with surface functionalization of amine groups. The ratio of powdered sample:DI water:glacial acetic:ethanol was 1:30:15:60. In this experiment, MCM-41(500 mg) of sample was mixed with DI water (15mL), glacial acetic (7.5 mL), and 75% ethanol (30 mL). The mixture was stirred for 10 minutes under room temperature, then 98% APTES (0.5 mL) was added, and stirred overnight. The sample was centrifuged (15,00 rpm, 10 min) and washed with DI water and ethanol. Solid sample was obtained after vacuum drying, named MCM-41-NH_2 (410 mg).

2.4. Fabrication Method of Mesoporous Silica Nanoparticles (MSNs)

At first, MCM-41-NH_2 (410 mg) was suspended in 40 mL of DI water and 0.4 mL of glutaraldehyde and stirred (4˚C, 1 h). Then, the mixture was centrifuged (12,000 rpm, 25˚C) for 10 minutes. The unreacted glutaraldehyde residue was further washed thrice with DI water and ethanol, and the supernatant was disposed of to eliminate toxicity concerns. The precipitate was vacuum-dried (60˚C, 24 h) and ground into powder. Chitosan (50 mg) was added to 30 mL of 0.1 M HCl under constant stirring at room temperature for 4 hours to obtain a chitosan solution. The prepared MCM-41-NH_2 powder (404 mg) was dispersed in the chitosan solution and stirred under two conditions: 1) 25˚C, 24 h; 2) 25˚C, 32 h. The sample was collected by centrifugation (15,000 rpm, 10 min) and was washed with DI water and ethanol followed by vacuum-dried overnight at 25˚C. The product was named MCM-41-CHIT (395 mg).

2.5. Characterization of Fabricated MCM-41 Products

2.5.1. X-Ray Diffractometer (XRD)

The crystalline and surface structure of both uncalcined and calcined MCM-41 and SBA-15 were characterized using XRD with 2-theta from 0 to 10 degrees.

2.5.2. Fourier-Transform Infrared Spectroscopy (FTIR)

FTIR was used to confirm the synthesis of uncalcined MCM-41, MCM-41, uncalcined SBA-15, SBA-15, and the grafting of functional groups like MCM-41-NH_2, and MCM-41-CHIT. The frequency range of FTIR spectral scanning was between 4000 and 500 cm^{-1}.

2.5.3. Scanning Electronic Microscope (SEM)

SEM images were obtained using a HITACHI S-4800 prototype model. Samples were prepared on a silica wafer then vacuum dried overnight. All samples were then coated with platinum before SEM imaging.

2.5.4. Brunauer-Emmett-Teller (BET) Surface Analysis

BET surface area analysis was given to MCM-4 (1 h), MCM-41 (2 h), SBA-15 (D3), SBA-15 (D7), MCM-41-NH_2, and MCM-41-CHIT. All samples (20 mg) were degassed prior to measurement, with the following condition: target temperature 120˚C, 5˚C /minute heating rate, soak time 960 minutes. After degassing, liquid nitrogen was used for adsorption-desorption surface analysis at −196˚C. The physisorption analysis lasted about 24 to 36 hours.

2.6. Drug Loading and Release

2.6.1. Dexamethasone (DEX) Loading onto Nanoparticles

Dexamethasone (20 mg) was added to 20 mL phosphate buffer saline (PBS) at pH 7.4. MCM-41, MCM-41- NH_2, MCM-41-CHIT, and SBA-15 (100 mg) were dissolved in the DEX-PBS solution. The solution was stirred (25˚C, 2 h). The supernatant was collected after centrifuge for analysis of loading efficiency. Further washing was conducted twice by adding PBS to the pellet and centrifuged (9000

rpm, 3 min at 25˚C).

2.6.2. Measuring Dexamethasone Loading Content

The absorbance of DEX in solution was measured using ultraviolet–visible spectrophotometer (UV-Vis, Model JASCO V-670) with the scanning wavelength range between 200 and 400 nm. The optical densities of the dexamethasone concentrations in different solutions were measured at 254 nm. Measurements were conducted three trials, and data presented is all in mean SD +/- 2 significant figures.

2.6.3. Calculating Loading Capacity and Loading Efficiency of Nanoparticles

To calculate the amount of dexamethasone encapsulated in MSNs, the prepared DEX@MCM-41, DEX@ MCM-41-NH_2, DEX@ MCM-41-CHIT, and DEX@SBA-15 solutions were centrifuged and washed with ethanol and water. The supernatants were carefully collected and measured at 254 nm using UV-Vis spectrophotometer. The absorption value of DEX in the supernatant was then measured. Loading capacity measures the maximum drug carrying ability in each nanocarrier. The loading capacity (LC%) of DEX were calculated using the following equation:

$$LC(\%) = \left[\left(M_0 - M_1 \right) / M \right] \times 100\%$$

Where M_0 is the total DEX mass added to each sample, M_1 is the DEX mass in the supernatant, M is the total mass of the nanoparticles without drugs.

Loading efficiency (LE%) measures the ratio between initial amount of drug added and the loaded drugs, following the below formula:

$$LE(\%) = \left[\left(D_l / D_t \right) \right] \times 100\%$$

Where D_l is the amount of drug loaded and D_t is the total amount of drug added to the nanoparticle mixture.

2.6.4. DEX Release from Nanoparticles

All DEX loaded samples were vacuum-dried at 60˚C for 24 h. Pellets of 30 mL PBS (pH 7.4), each with 100 mg of DEX@MCM-41, DEX@ MCM-41-NH_2, DEX@ MCM-41-CHIT, and DEX@SBA-15 respectively, were put into water bath shaker and then shaken (100 rpm at 25˚C) for 21 days under dark conditions. At scheduled time intervals (0.5, 1, 2, 4, 6, 8, 12, 24h, 2d, 3d, 4d,…, 19d, 20d, 21d), 4 ml of the PBS solution was collected from each pellet for further analysis. To maintain a constant volume, the withdrawn amount was returned, after each measurement, to the release media to keep a constant cumulative release percentage. Measurements were conducted three trials, and data presented is all in mean SD +/- 2 significant figures.

2.6.5. Calculating Cumulative Release Percentage (%)

To calculate the amount of dexamethasone released from the prepared DEX@MCM-41, DEX@ MCM-41-NH_2, DEX@ MCM-41-CHIT, and DEX@SBA-15 solutions, the collected sample solutions in different time periods were meas-

ured at 254 nm by UV-Vis spectrophotometer.

The cumulative release (CR%) of DEX was calculated using the following equation:

$$CR(\%) = (D_r / D_l) \times 100\%$$

where D_r is the total DEX mass released, D_l is the total DEX mass loaded.

2.7. Constructing Mathematical Models

To predict long-term release kinetics of dexamethasone from different nanocarriers, mathematical models were constructed to find the drug release pattern and equations. The 7-day release data from DEX@MCM-41, DEX@ MCM-41-CHIT, and DEX@SBA-15 were used to construct mathematical models. DD-solver extension in Microsoft Excel was used to construct models [20]. Sample drug release models included: zero-order, first order, Higuchi, and Korsmeyer-Peppas (KP).

3. Results and Discussions

3.1. Characterization of MSN Samples

3.1.1. XRD Patterns of MCM-41 and SBA-15

In this work, the ordered mesoporous structure of the silica nanoparticles was confirmed by small angle XRD measurement. The 2θ positions corresponded to the spacing between the crystals or atoms. The height of the peaks showed a greater intensity, representing the amount of molecules within that spacing. For MCM-41 (**Figure 4**), the findings revealed that a broad diffraction peak was emerged at 2θ = 2.4˚ representing the reflections of the ordered two-dimensional hexagonal mesoporous structure. Three well-defined diffraction peaks (100), (110) and (200) were clearly observed in the XRD pattern. The thickness of pore walls also correlated with the peak intensities. The decreased relative intensity of (200) peak to the (110) peak revealed the decrease in the thickness of the pore wall in MCM-41 as compared to MCM-41-CTAB. The diffraction pattern of MCM-41 type MSN represented the hexagonal mesoporous structure with 2 - 4 nm in pore size and 0.6 - 1.2 nm in wall thicknesses. The (100) diffraction peak of MCM-41 became flatter after calcination, showing a slight damage of 3D structure of the hexagonal nanoparticle body due to long-term exposure under high heat. For SBA-15, small-angle XRD confirms the hexagonally-ordered porous structure by displaying three well-resolved peaks assigned as the (100), (110) and (200) planes (**Figure 5**). The 2θ peaks in SBA-15 were relatively smaller than MCM-41, indicating bigger pore size.

3.1.2. FTIR Spectra

FTIR spectra for MCM-41-CTAB (**Figure 6**) showed the band at 1084 - 1230 cm^{-1}, which demonstrated silica composite formation. Complete removal of the surfactant CTAB from the MSNs was confirmed by the disappearance of the wide absorption C–H peak at 2810 cm^{-1}.

FTIR spectra for MCM-41, MCM-41-NH_2, and MCM-41-CHIT (**Figure 7**) displayed transmission peaks at about 1075 cm^{-1} and 800 cm^{-1}, which were assigned

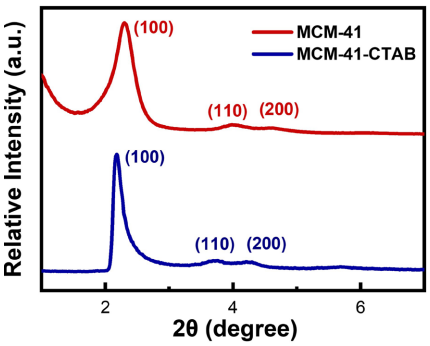

Figure 4. XRD patterns of uncalcined and calcined MCM-41.

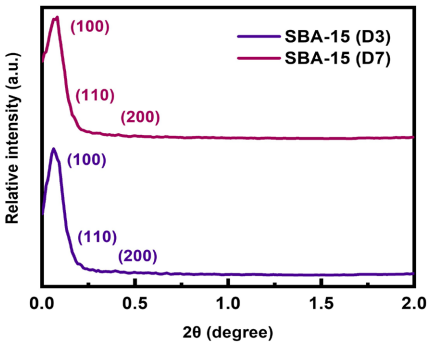

Figure 5. XRD patterns of SBA-15.

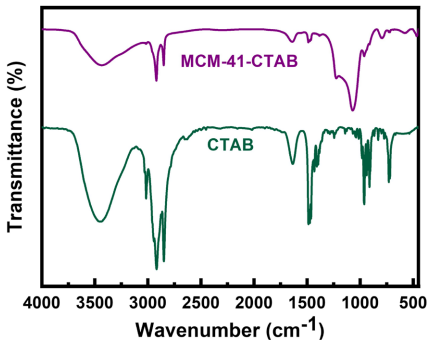

Figure 6. FTIR spectra of uncalcined and calcined MCM-41.

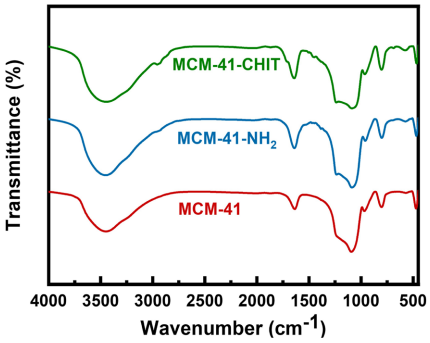

Figure 7. FTIR spectra of MCM-41, MCM-41-NH_2, and MCM-41-CHIT.

to the characteristic stretching vibrations of the Si-O bond. The corresponding fingerprints of aminopropyl functional groups of APTES was confirmed by the presence of a new band at around 1554 cm^{-1} related to asymmetric NH_2 bending. In addition, the increased specific band of MCM-41-CHIT could be attributable to the alkyl groups of C-H bond by the weak C–H stretching vibrations at 2980 cm^{-1}. In reviewed literature, the spectrum of the MSN-APTES-chitosan sample would show two bands at 1467 cm^{-1} and 1633 cm^{-1} associated with amino groups in biopolymer chains with N-H and C-N bonding [15]. It showed a trivial curve in our result.

3.1.3. SEM Images of MSN Samples

The particle size and the size distribution of synthesized MSNs were analyzed using SEM. The morphology of the MCM-41 using SEM technique showed spherical shapes (**Figure 8**). MCM-41 (60˚C, 1 h) particles aggregated heavier and tighter than MCM-41 (80˚C, 2 h).

The particle size was measured by the SEM images (**Figure 9**). MCM-41 nanoparticles exhibited an average size of 95.1 nm. MCM-41-NH_2 nanoparticles exhibited an average size of 82.2 nm. MCM-41-CHIT nanoparticles exhibited an average size of 110 nm with uniform size and shape.

From the SEM image shown (**Figure 10**), the extracted SBA-15 materials were

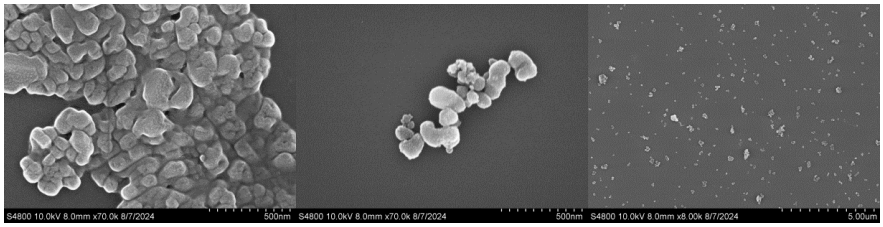

Figure 8. SEM of MCM-41.

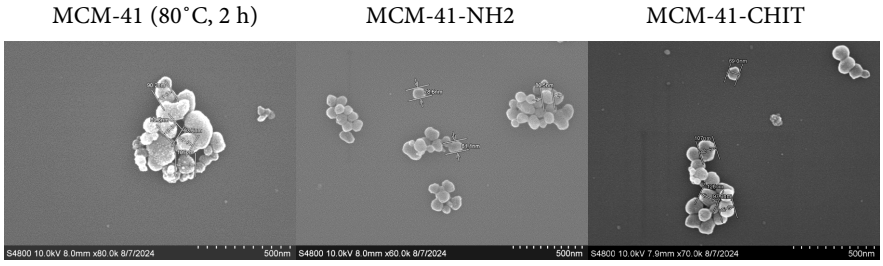

Figure 9. SEM of functionalized MCM-41 species

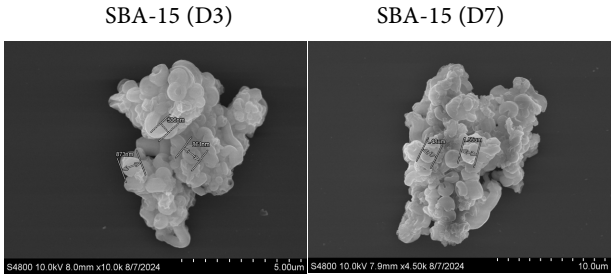

Figure 10. SEM of SBA-15.

aggregated into wheatlike macrostructures. The particle diameter of SBA-15 was around 1 μm. The particle size of SBA-15(D7) was relatively larger than SBA-15(D3).

3.1.4. BET Surface Area Analysis of MSN Samples

The nitrogen adsorption and desorption isotherms of MCM-41, MCM-41-NH_2, and MCM-41-CHIT were shown (Figure 11). All adsorption/desorption patterns of all materials follow the pattern of mesoporous nanomaterials, proving MSNs to be mesoporous. Analysis of the nitrogen adsorption/desorption isotherms yielded BET specific surface areas of approximately 896 m^2/g in MCM-41, 619 m^2/g in MCM-41-NH_2, 519 m^2/g in MCM-41-CHIT, 1027 m^2/g in SBA-15 (D3), and 999 m^2/g in SBA-15 (D7). The pore volumes were 1.03 cm^3/g in MCM-41, 0.88 cm^3/g in MCM-41-NH_2, and 0.82 cm^3/g in MCM-41-CHIT (Figure 12).

Comparing MCM-41 and SBA-15, SBA-15 has significantly greater specific surface area and pore volume. This is attributed to the surfactant template used in each nanoparticle assembly. Cationic CTAB was used as surfactant template for MCM-41. In a slightly basic liquid environment, CTAB molecules self-arrange and congregate into micelles, with hydrophobic tails clustered at the center of each micelle. Hexagonal prism structures were formed, so-called the hexagonal close-packed structure of MCM-41 [15]-[17]. While SBA-15 has similar structure than MCM-41, its surfactant template, P-123, is a triblock copolymer template [21] [22]. Unlike cationic surfactants, which self-arrange via ion-dipole interaction,

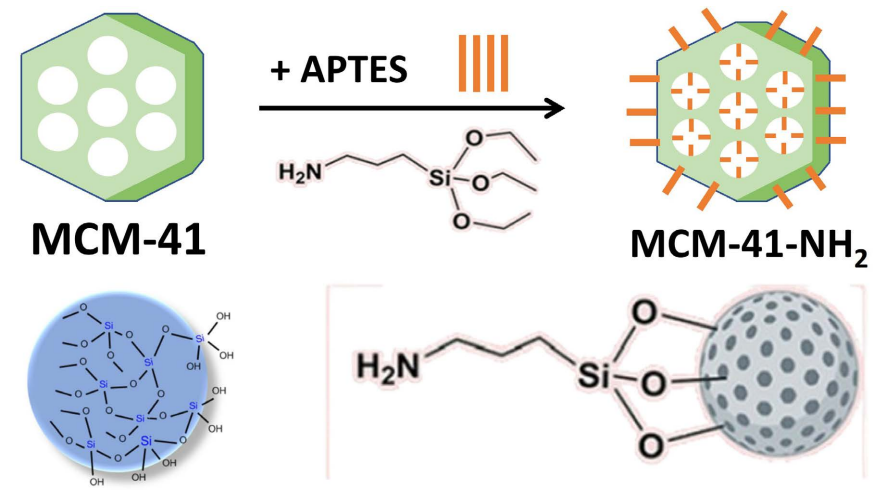

Figure 11. Amine grafting onto MCM-41.

Figure 12. Chitosan encapsulation around MCM-41.

copolymer exhibits a weaker dipole-dipole interaction, forming bigger, more dispersed pores [21]-[23]. Furthermore, the average particle size of CTAB is 0.263 nm^3, while P123 is 9.461 nm^3. The different sizes of surfactant templates result in differences in surface area, pore volume, pore diameter, wall thickness, and pore dispersity.

Comparing MCM-41-NH_2 and MCM-41 (Figure 13), the prior decreased in specific surface area. This is attributed to the amine grafting on the surface of MCM-41 and inside the pores. After chitosan coating, the nitrogen adsorption isotherms of MCM-41-CHIT showed a relatively flat isotherm, accompanied by a loss of hysteresis loop. The surface area of MCM-41-CHIT decreased and the particle diameters increased. Pore volume remained constant after chitosan coating, proving chitosan only coated the exterior of spherical nanoparticles (Figure 14). Chitosan caps around the nanoparticle, acting as gatekeeper and additional loading platform.

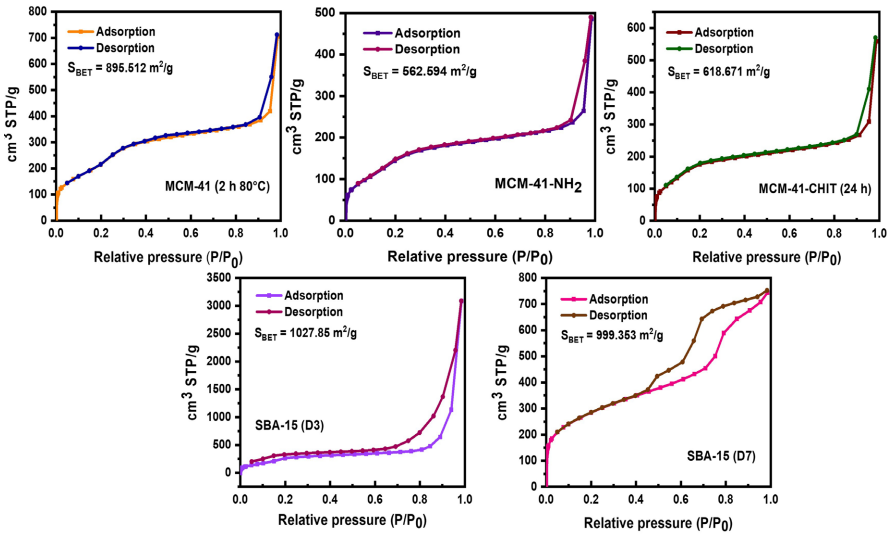

Figure 13. N_2 adsorption/desorption isotherms of functionalized MSN samples.

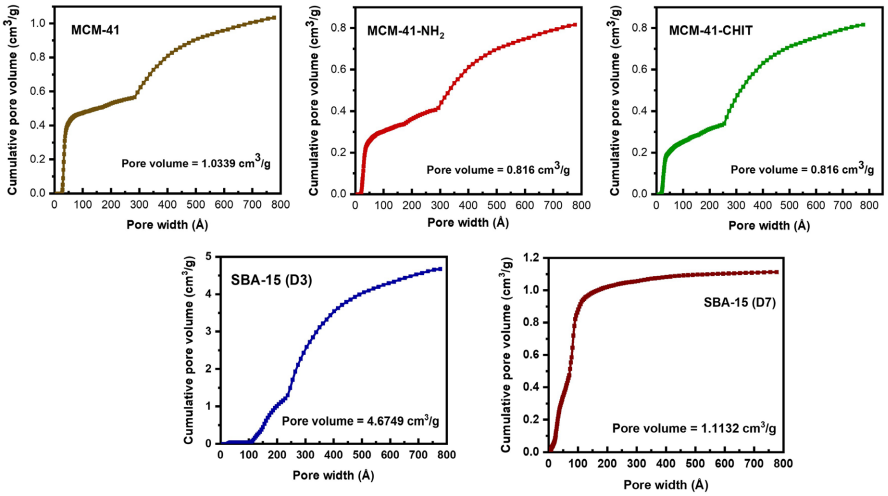

Figure 14. BET pore volume analysis of functionalized MSN samples.

3.2. Dexamethasone Loading

UV-Vis spectroscopy is a powerful tool for analyzing specific chemical compounds by quantifying ultraviolet beam pathways, with each unique compound matching with a specific wavelength. According to Beer-Lambert Law, each molecule had a unique molar absorptivity, producing different absorbance.

20 mg of DEX was loaded onto 100 mg of MCM-41, MCM-41-NH_2, and MCM-41-CHIT in 20 ml PBS solution respectively. Control group was prepared with 20 mg of DEX in 20 ml PBS solution (pH = 7.4). The concentration of DEX in the supernatant after centrifuge was quantified by UV-Vis spectrometer. The peaks present at 254 nm for DEX@MCM-41, DEX@ MCM-41-NH_2, and DEX@ MCM-41-CHIT indicated a successful loading of DEX (Figure 15). The concentrations of DEX were calculated by Beer-Lambert Law (Table 2). The loading capacity of MCM-41-CHIT showed 54.5%, followed by 34.9% in MCM-41-NH_2 and 27.9% in MCM-41 (Figure 16). Loading efficiency was determined. The loading efficiency of MCM-41-CHIT showed 26.9%, followed by 17.5% in MCM-41-NH_2 and 14% in MCM-41 (Figure 17). MCM-41 had almost twice the loading capacity and efficiency of MCM-41, showing great improvement of drug loading with chitosan functionalization on the surface of nanocarrier. The results demonstrated a promising effect of the chitosan modification which showed higher loading efficiency than non-modified MSN. The speculation below was in accordance with the experimental results. In order to achieve high loading efficiency for DEX, it is necessary to induce specific and strong interactions between the surface of the silica carrier and DEX molecules. Functionalizing the surface of the MSNs with chitosan could enhance the interaction with DEX molecules by forming multiple hydrogen bonds for stronger intermolecular forces.

Chitosan not only acts as an excellent drug loading platform, but a great biopolymer with high affinity with mucus membranes in the body. It is a plurivalent biopolymer due to its multiple amino groups, high affinity, positive charges, and chain-like structure [19] [24]. In the experiment, based on the absorbance ratio of

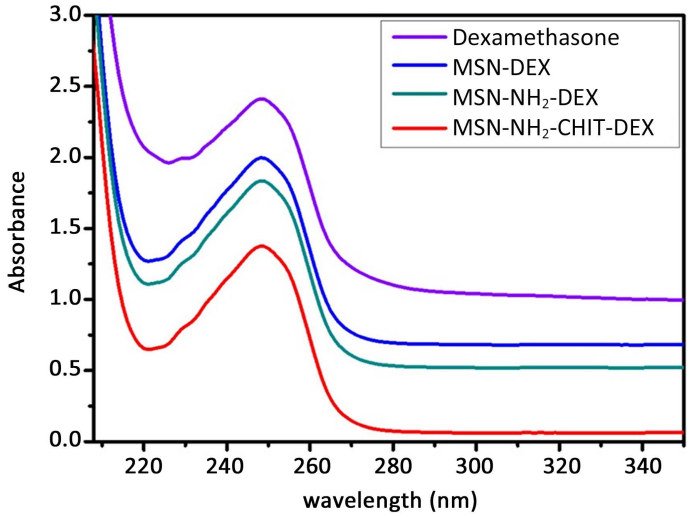

Figure 15. UV-vis spectrophotometer absorbance spectra of nanoparticles.

Table 2. Calculated concentration of DEX in each nanoparticle sample.

	DEX(μg/ml)
DEX	2.72
DEX@MCM-41	1.96
DEX-MCM-41-NH_2	1.77
DEX@MCM-41-CHIT	1.26

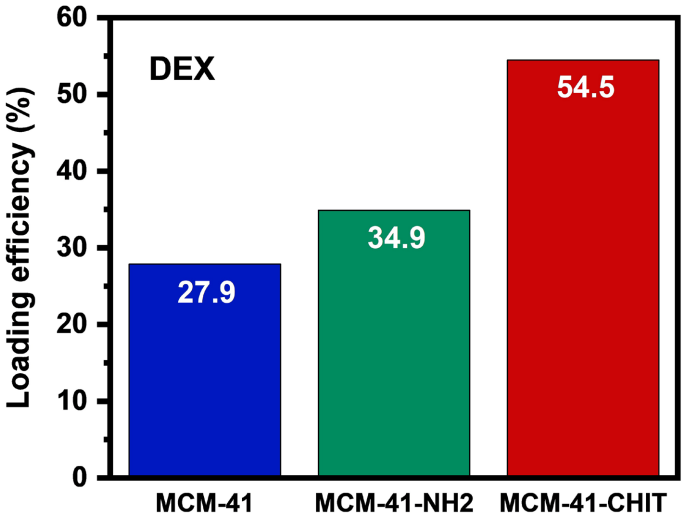

Figure 16. Loading capacity of nanoparticles.

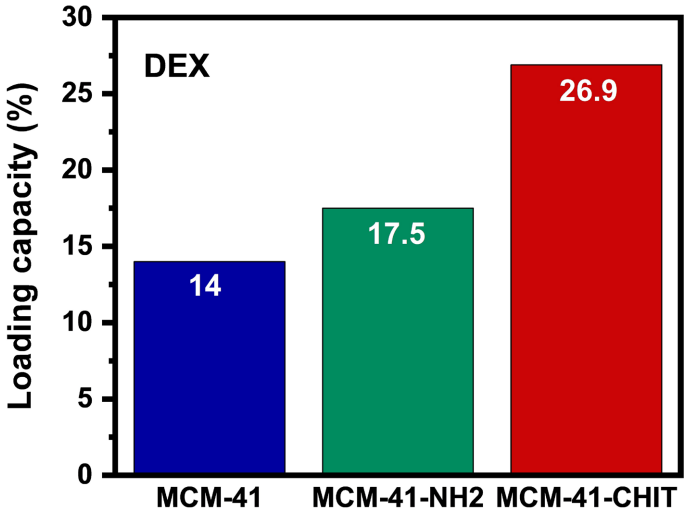

Figure 17. Loading efficiency of DEX onto nanoparticles.

the amino groups and hydroxyl groups from FTIR spectrum data, the degree of acetylation (DDA) was calculated using the below formula [24]:

$$DDA(\%) = \left(1 - \left(A_{\text{amino}} / A_{\text{hydroxyl}}\right) / 1.33\right) \times 100$$

Where A_{amino} is the absorbance band of amino group at 1655 cm^{-1}, A_{hydroxyl} is the absorbance band of hydroxyl group at around 3450 cm^{-1}, and 1.33 is the ratio

between fully N-acetylated chitosan. In this experiment, the standard deacetylation procedure was not performed, but the DDA was speculated to be around 88% based on FTIR data. A high DDA indicates more free amino groups resulted from the alkali treatment, resulting in more positive charges, thus forming a stronger affinity with mucus membranes.

3.3. Dexamethasone Release

The release kinetics of dexamethasone from DEX@MCM-41, DEX@ MCM-41-NH_2, DEX@ MCM-41-CHIT, DEX@SBA-15 (D3), and DEX@SBA-15 (D7) in PBS buffer at pH 7.4 were shown (**Figure 18**). The graphic pattern showed that the release in DEX@MCM-41 and DEX@ MCM-41-NH_2 already reached around 50% at 12 h and then around 80% at 48 h and revealed a fast drug release profile, so-called "burst release". Then it showed a ceasing trend of DEX release as indicated by the flat plateau from 48 to 120 h, indicating that both carriers reached a release terminal. On the other hand, DEX@ MCM-41-CHIT released only 5% at 12 h and reached 10% at 48 h. The release was slowly sustained throughout the time intervals in 120h, which showed linearly constant release profile. The predictable drug release in constant rate was an essential factor for the drug delivery system to maintain a stable therapeutic effect at target tissue site.

The cumulative release from dispersed DEX@MCM-41, DEX@ MCM-41-NH_2, and DEX@ MCM-41-CHIT reached 90.7%, 87.3% and 19.3% respectively (**Figure 18(B)**). In DEX@MCM-41 and DEX@ MCM-41-NH_2, the DEX molecules were loaded in the pores via weak intermolecular forces. The release began with the diffusion process of incorporated drug from the mesoporous channels toward the PBS media. This diffusion process was triggered immediately after the contact of the nanocarriers with the aqueous media. As a result, the DEX molecules easily diffused out of the pores, resulting in large amount premature release in short period of time.

In order to maintain drug release in slow and constant rate, chitosan was capped around MCM-41 to control the DEX release, acting as a gatekeeper. Through cross-linking reaction with glutaraldehyde under acidic environment, chitosan molecules formed a shell-like cap on the exterior MSN (**Figure 19**). DEX molecules embedded in the MSN pore channels were kept in by chitosan, thus unlikely to escape with the effusion process.

3.4. Mathematical Model to Simulate Drug Release Pattern of MSNs

The equations for drug release models applied to this experiment were shown (**Table 3**). Below model were applied to the 7-day release data from DEX@MCM-41, DEX@MCM-41-CHIT, and DEX@SBA-15. Model suitability were judged based on the adjusted R-squared value (R^2 adj.) (**Table 4**).

First-order, Higuchi, and KP models were applied to DEX@MCM-41 (**Figure 20**). MCM-41 exhibited a burst release in the first 48 hours followed by decreased release rate in the following days. This behavior was best simulated by first-order

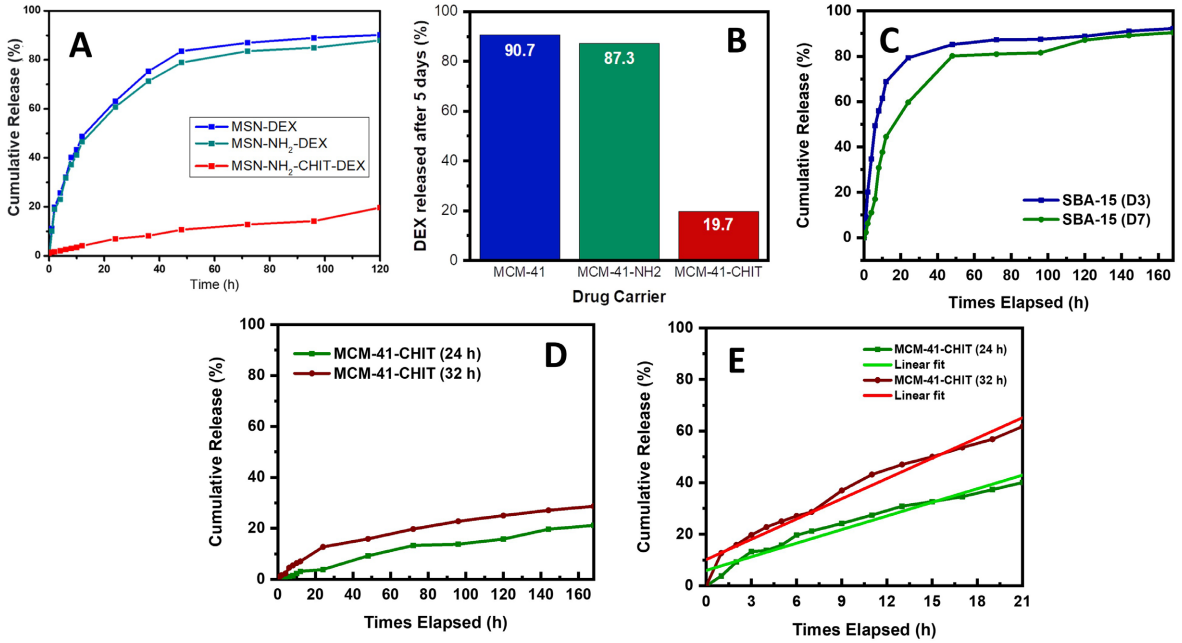

Figure 18. (A) release kinetics of DEX@MCM-41, DEX@ MCM-41-NH_2, DEX@ and MCM-41-CHIT; (B) released amount of DEX from MCM-41, MCM-41NH_2, MCM-41-CHIT; (C) release kinetics of DEX@SBA-15 (D3) and DEX@SBA-15 (D7); (D) release comparison between DEX@MCM-41-CHIT; E) linear fit model of MCM-41-CHIT drug release.

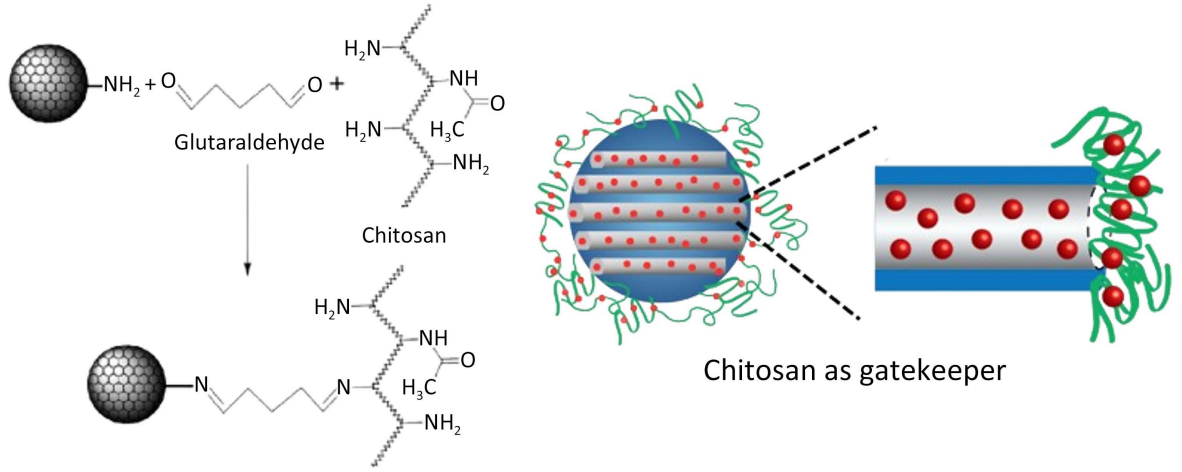

Figure 19. Schematic illustration demonstrating chitosan's mechanism as gatekeeper on MSN surface.

Table 3. Drug release models with equations.

Models	Equations
Zero-order	$Q_t = Q_0{}^*K$
First-order	$Q_t = Q_0 e^{-Kt}$
Higuchi	$Q = K_H t^{1/2}$
Korsmeyer-Peppas	$Q_t/Q\infty = K_k t^n$

Qt: amount of drug release at time t, Q: cumulative drug release at time t, Q∞: drug released at infinite time (maximum hypothetical release), K: release rate constant found by model fitting: KH: constant of Higuchi model; Kk: constant of KP model, n: release exponent indicating rate of release

Table 4. R^2 adj. values for release models.

Nanocarrier	Math model	R^2 adj. values	Important values
DEX@MCM-41	First-order	0.9670	K = 0.058
	Higuchi	0.8231	K_H = 9.256
	Korsmeyer-Peppas	0.9532	K_k = 21.39; n = 0.313
DEX@SBA-15 (D3)	First-order	0.9330	K = 0.097
	Higuchi	0.4782	K_H = 9.310
	Korsmeyer-Peppas	0.8779	K_k = 30.945; n = 0.231
DEX@MCM-41-CHIT	First-order	0.9779	K = 0.002
	Higuchi	0.9329	K_H = 1.455
	Korsmeyer-Peppas	0.9887	K_k = 0.428; n = 0.466

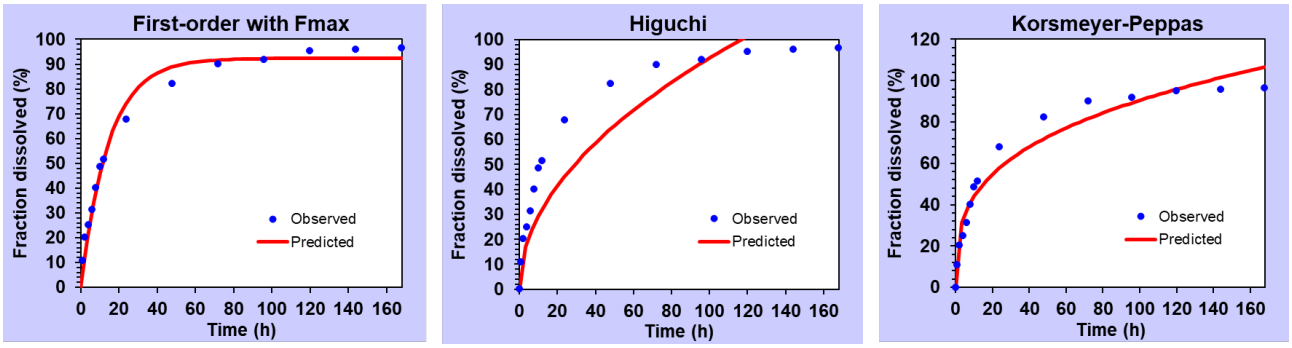

Figure 20. Drug release models on DEX@MCM-41.

model, with and R^2 adjusted value of 0.9670 (Table 4). In a first-order equation, the rate of change of dependent variable is directly proportional to the independent variable. In the release amount is directly affected by the initial amount of drugs added. This pattern was observed in from MCM-41 because the carrier had weak binding force between DEX molecules and nanocarriers. Since carriers fail to hold drug molecules in place and control their release, the more drugs added in the beginning, the more would burst release out. From 48th to 168th hour, MCM-41 releases at a decreasing because the drug molecules stuck on the surface were mostly released, and the ones that fitted in the pores released out slowly. The same pattern applied to DEX@SBA-15, with the first-order model having the highest R^2 value of 0.9330 (Figure 21) (Table 4).

On the other hand, the 7-day release of DEX@MCM-41-CHIT fits Korsmeyer-Peppas model due to it being a polymetric system release (Figure 22). KP model is normally used to simulate release from polymeric surface, nanoparticles, or hydrogel because the model measures the release ratio instead of precise release amount [25]. The ratio-based calculation allows more margin of error and flexibility at each release interval [25]. The R^2 value of was 0.9887. In the KP model, the n value indicates the drug release mechanism. When $n < 0.45$, it is a Fickian diffusion; if $0.45 < n < 0.89$, it is a non-standard release. In this experiment, all

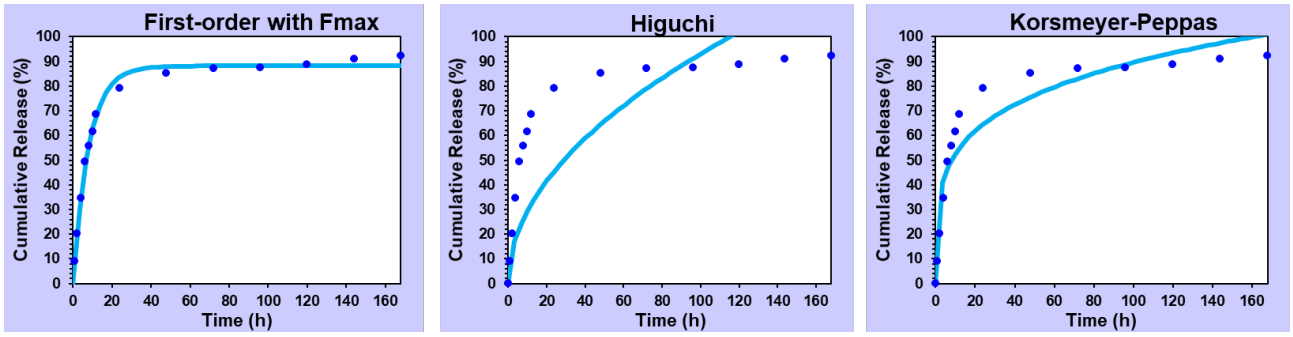

Figure 21. Drug release models on DEX@SBA-15 (D3).

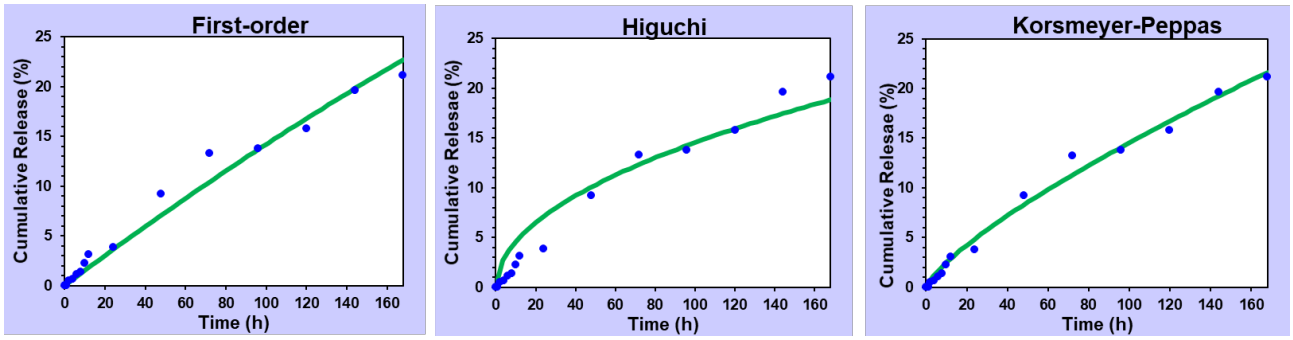

Figure 22. Drug release models on DEX@MCM-41-CHIT.

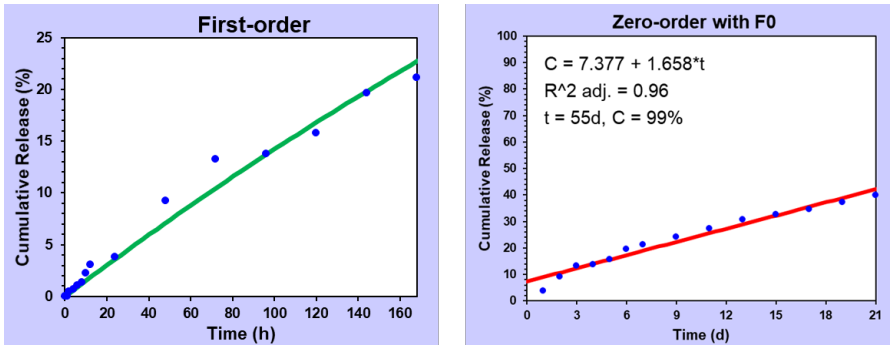

Figure 23. 7-day V.S.21-day release simulation.

three DEX@MCM-41, DEX@SBA-15, and DEX@MCM-41-CHIT all fitted an n value of < 0.45. Hence, in the first 168 hours, the release mechanism could be seen as a Fick's diffusion, which states that diffusion flux correlates positively with the concentration gradient of particle [25] [26].

When comparing the 7-day release and 21-day release of DEX@MCM-41-CHIT, the most suitable model became zero-order, with an R^2 value of 0.960 (**Figure 23**). Zero-order model is not affected by the initial drug amount nor the hypothetical maximum release. In a zero-order release, the amount of drug released at each interval remains constant. On average, DEX@MCM-41-CHIT released 1.658% of loaded drugs per day, which was about 0.2 mg, just under the recommended prescription for inflammation treatment. According to the model's prediction, it would take around 55 days for all of the loaded drugs to release. To

match the recommended prescription for treating inflammation, the initial amount of drug loaded would have to increase to 100 mg.

4. Conclusions

In this study, we achieved a successful approach to improve the dexamethasone treatment of lung disease via a smart mucoadhesive drug delivery system. The MCM-41 and SBA-15 type mesoporous silica nanoparticles were optimized through various synthesis conditions and the verification of characterization. Functionalization of MCM-41 with chitosan was performed through two-step conjugations of APTES amination and glutaraldehyde crosslinking. Dexamethasone was loaded in the MCM-41-CHIT and showed a high loading capacity of 53.7%. Accumulative release profile of dexamethasone in physiological solution showed the linear relationship of a constant rate for a serial period of time. The release in 120 hours was 19.7% for MCM-41-CHIT.

Mathematical models were fitted to each release pattern of each nanocarrier. MCM-41 and SBA-15 both fitted the first-order model, indicating their release mechanism followed a diffusion process and was affected by the initial loaded amount. MCM-41-CHIT fitted the zero-order model, proving its constant and consistent release every day with a potential of completing a 55-day release. Overall, these results suggested that the chitosan capped MSN could be a suitable candidate as a DEX carrier for mucoadhesive drug delivery over long-term treatment.

Conflicts of Interest

The authors declare no conflicts of interest regarding the publication of this paper.

References

[1] WHO (2025) Coronavirus Disease (COVID-19). https://www.who.int/health-topics/coronavirus

[2] Recovery Collaborative Group, Horby, P., Lim, W.S., Emberson, J.R., Mafham, M., Bell, J.L., *et al.* (2021) Dexamethasone in Hospitalized Patients with Covid-19. *New England Journal of Medicine*, **384**, 693-704. https://doi.org/10.1056/nejmoa2021436

[3] Li, A.F.Y., Wang, C.L., Tai, H.Y., Fu, Y.J., Tsai, F.T., Tsai, Y.C., *et al.* (2021) Pandemic Aspect of Dexamethasone: Molecular Mechanisms and Clinical Application. *Journal of the Chinese Medical Association*, **84**, 245-247. https://doi.org/10.1097/jcma.0000000000000485

[4] Johnson, D.B., Lopez, M.J. and Kelley, B. (2025) Dexamethasone. StatPearls Publishing.

[5] Vardy, J., Chiew, K.S., Galica, J., Pond, G.R. and Tannock, I.F. (2006) Side Effects Associated with the Use of Dexamethasone for Prophylaxis of Delayed Emesis after Moderately Emetogenic Chemotherapy. *British Journal of Cancer*, **94**, 1011-1015. https://doi.org/10.1038/sj.bjc.6603048

[6] Polderman, J.A., Farhang-Razi, V., Van Dieren, S., Kranke, P., DeVries, J.H., Hollmann, M.W., *et al.* (2018) Adverse Side Effects of Dexamethasone in Surgical Patients. *Cochrane Database of Systematic Reviews*, **11**, CD011940. https://doi.org/10.1002/14651858.cd011940.pub3

[7] Amin, M.K. and Boateng, J.S. (2022) Enhancing Stability and Mucoadhesive Properties of Chitosan Nanoparticles by Surface Modification with Sodium Alginate and Polyethylene Glycol for Potential Oral Mucosa Vaccine Delivery. *Marine Drugs*, **20**, Article 156. https://doi.org/10.3390/md20030156

[8] Vaezi Moghaddam, A., Mortazavi, S.A., Kobarfard, F., Bafkary, R. and Darbasizadeh, B. (2023) Synthesis and Functionalization of Mucoadhesive Mesoporous Silica Particles Containing Diphenhydramine for Treatment of Aphthous Ulcers. *BioImpacts*, **13**, 456-466. https://doi.org/10.34172/bi.2023.27548

[9] Sharma, R., Kumar, S., Malviya, R., Prajapati, B.G., Puri, D., Limmatvapirat, S., *et al.* (2024) Recent Advances in Biopolymer-Based Mucoadhesive Drug Delivery Systems for Oral Application. *Journal of Drug Delivery Science and Technology*, **91**, Article 105227. https://doi.org/10.1016/j.jddst.2023.105227

[10] Harris, D. and Robinson, J.R. (1992) Drug Delivery via the Mucous Membranes of the Oral Cavity. *Journal of Pharmaceutical Sciences*, **81**, 1-10. https://doi.org/10.1002/jps.2600810102

[11] Dobbs, E.C. (1963) Drugs Which Act on the Skin and Mucous Membranes. *Dental Clinics of North America*, **7**, 473-487. https://doi.org/10.1016/s0011-8532(22)02061-4

[12] Sato, H. (2025) Development of Nanoparticle-Based Mucosal Drug Delivery Systems for Controlling Pharmacokinetic Behaviors. *Biological and Pharmaceutical Bulletin*, **48**, 759-768. https://doi.org/10.1248/bpb.b25-00071

[13] Yan, X. and Sha, X. (2023) Nanoparticle-Mediated Strategies for Enhanced Drug Penetration and Retention in the Airway Mucosa. *Pharmaceutics*, **15**, Article 2457. https://doi.org/10.3390/pharmaceutics15102457

[14] Zheng, B., Liu, D., Qin, X., Zhang, D. and Zhang, P. (2025) Mucoadhesive-to-Mucopenetrating Nanoparticles for Mucosal Drug Delivery: A Mini Review. *International Journal of Nanomedicine*, **20**, 2241-2252. https://doi.org/10.2147/ijn.s505427

[15] Kankala, R.K., Han, Y., Na, J., Lee, C., Sun, Z., Wang, S., *et al.* (2020) Nanoarchitectured Structure and Surface Biofunctionality of Mesoporous Silica Nanoparticles. *Advanced Materials*, **32**, Article 1907035. https://doi.org/10.1002/adma.201907035

[16] Pongchaikul, P., Hajidariyor, T., Khetlai, N., Yu, Y., Arjfuk, P., Khemthong, P., *et al.* (2023) Nanostructured N/S Doped Carbon Dots/Mesoporous Silica Nanoparticles and PVA Composite Hydrogel Fabrication for Anti-Microbial and Anti-Biofilm Application. *International Journal of Pharmaceutics: X*, **6**, Article 100209. https://doi.org/10.1016/j.ijpx.2023.100209

[17] Gómez, L., Rivero-Buceta, E.M., Vidaurre-Agut, C. and Botella, P. (2025) Preparation of Mesoporous Silica Nanoparticles by Spray Drying. *Microporous and Mesoporous Materials*, **393**, Article 113646. https://doi.org/10.1016/j.micromeso.2025.113646

[18] Ways, T.M.M., Lau, W. and Khutoryanskiy, V. (2018) Chitosan and Its Derivatives for Application in Mucoadhesive Drug Delivery Systems. *Polymers*, **10**, Article 267. https://doi.org/10.3390/polym10030267

[19] Ahmad, K., Zhang, Y., Chen, P., Yang, X. and Hou, H. (2024) Chitosan Interaction with Stomach Mucin Layer to Enhances Gastric Retention and Mucoadhesive Properties. *Carbohydrate Polymers*, **333**, Article 121926. https://doi.org/10.1016/j.carbpol.2024.121926

[20] Zhang, Y., Huo, M., Zhou, J., Zou, A., Li, W., Yao, C., *et al.* (2010) Ddsolver: An Add-In Program for Modeling and Comparison of Drug Dissolution Profiles. *The AAPS Journal*, **12**, 263-271. https://doi.org/10.1208/s12248-010-9185-1

[21] Albayati, T.M., Salih, I.K. and Alazzawi, H.F. (2019) Synthesis and Characterization of a Modified Surface of SBA-15 Mesoporous Silica for a Chloramphenicol Drug Delivery System. *Heliyon*, **5**, e02539. https://doi.org/10.1016/j.heliyon.2019.e02539

[22] Thahir, R.W., Wahab, A.L., Nafie, N. and Raya, I. (2019) Synthesis of Mesoporous Silica SBA-15 through Surfactant Set-Up and Hydrothermal Process. *Rasayan Journal of Chemistry*, **12**, 1117-1126.

[23] Larki, A., Saghanezhad, S.J. and Ghomi, M. (2021) Recent Advances of Functionalized SBA-15 in the Separation/Preconcentration of Various Analytes: A Review. *Microchemical Journal*, **169**, Article 106601. https://doi.org/10.1016/j.microc.2021.106601

[24] Dabija, M.G., Olaru, I., Ciuhodaru, T., Stefanache, A., Mihai, C., Lungu, I.I., *et al.* (2025) Chitosan as a Plurivalent Biopolymer in Nanodelivery Systems. *Polymers*, **17**, Article 558. https://doi.org/10.3390/polym17050558

[25] Heredia, N.S., Vizuete, K., Flores-Calero, M., Pazmiño V., K., Pilaquinga, F., Kumar, B., *et al.* (2022) Comparative Statistical Analysis of the Release Kinetics Models for Nanoprecipitated Drug Delivery Systems Based on Poly (Lactic-Co-Glycolic Acid). *PLOS ONE*, **17**, e0264825. https://doi.org/10.1371/journal.pone.0264825

[26] Dash, S., Murthy, P.N., Nath, L. and Chowdhury, P. (2010) Kinetic Modeling on Drug Release from Controlled Drug Delivery Systems. *Acta Poloniae Pharmaceutica*, **67**, 217-223.